Quantifying net community production and calcification at Station ALOHA near Hawai'i: Insights and limitations from a dual tracer carbon budget approach

Lucie A. C. M. Knor[1], Christopher L. Sabine[1], Adrienne J. Sutton[2], John Dore[3], Angelicque E. White[1], James Potemra[1], and Robert A. Weller[4]

[1]University of Hawai'i at Mānoa, Honolulu, Hawai'i, USA

[2]NOAA Pacific Marine Environmental Laboratory, Seattle, Washington, USA

[3]Montana State University, Bozeman, Montana, USA

[4]Woods Hole Oceanographic Institution, Falmouth, Massachusetts, USA

Corresponding author: Lucie Anna Christa Maria Knor (luciek@hawaii.edu)

Key Points:

- First calculation of community calcification with a budget approach at this location, results exceed reported sediment trap data.
- Calculated net community production confirms net autotrophy over a year, on the lower end of previous estimates.
- It is important to better constrain physical, especially horizontal, transport of carbon to further investigate mixed layer carbon cycling.

Abstract

A budget approach is used to disentangle drivers of the seasonal mixed layer carbon cycle at Station ALOHA (A Long-term Oligotrophic Habitat Assessment) in the North Pacific Subtropical Gyre (NPSG). The budget utilizes data from the WHOTS (Woods Hole - Hawaii Ocean Time-series Site) mooring, and the ship-based Hawai‘i Ocean Time-series (HOT) in the North Pacific Subtropical Gyre (NPSG), a region of significant oceanic carbon uptake. Parsing the carbon variations into process components allows an assessment of both the proportional contributions of mixed layer carbon drivers, and the seasonal interplay of drawdown and supply from different processes. Annual net community production reported here is at the lower end of previously published data, while net community calcification estimates are 4- to 7-fold higher than available sediment trap data, the only other estimate of calcium carbonate export at this location. Although the observed seasonal cycle in dissolved inorganic carbon (DIC) in the NPSG has a relatively small amplitude, larger fluxes offset each other over an average year, with major supply from physical transport, especially lateral eddy transport throughout the year and entrainment in the winter, and biological carbon uptake in the spring. Gas exchange plays a smaller role, supplying carbon to the surface ocean between Dec-May, and outgassing in Jul-Oct. Evaporation-precipitation (E–P) is variable with precipitation prevailing in the first- and evaporation in the second half of the year. The observed total alkalinity signal is largely governed by E–P, with a somewhat stronger net calcification signal in the wintertime.

Plain Language Summary

The ocean carbon cycle is a complicated system. In it, chemical compounds react, are moved by ocean physics, altered by organisms, and exchange with CO_2 in the atmosphere. To explore how the ocean will continue to take up CO_2 from the atmosphere, and how much will be removed into the deep ocean, we need to know how these processes influence ocean carbon. Here, we investigate them over a year. We create a model from observations of two carbon compounds, together with calculated estimates of processes (evaporation and precipitation, transport through the water, and air-sea exchange) to back out the influence of two important reaction pairs executed by organisms: Photosynthesis and respiration, and calcification and dissolution. Over a year, the surface community at this location near Hawai‘i in the Pacific photosynthesizes more than it respires, removing 66 grams of CO_2 per square meter. Also, marine calcifyers perform calcification, and our estimates are much higher than previous measurements from sediment traps. Gas exchange and evaporation-precipitation vary with the seasons in opposite directions, and there are carbon inputs from horizontal transport throughout the year, and from water column mixing in the winter.

1 Introduction

1.1 Rationale

The biological pumps are a fundamental component of the global carbon cycle, driving the transfer of carbon from the atmosphere to the deep ocean. Multiple surface ocean processes play a role in carbon concentrations and export from the mixed layer, including physical (gas exchange, evaporation and precipitation, advection, vertical mixing) and biogeochemical processes, namely photosynthesis, respiration, calcification, and dissolution (Figure 1). Impacts on biological pumps of changing ocean conditions, such as warming, increased stratification, or ocean acidification due to climate change, could significantly alter marine carbon cycling, as well as removal and sequestration of atmospheric CO_2 through various (potential) feedback loops. This includes the potential for shifts in community structure as ecosystems respond to changing chemistry, enhanced recycling in a warmer surface ocean, or reduced particle ballasting and calcification, which all impact carbon export (Sabine & Tanhua, 2010). Consequently, we need to quantify changes in the mixed layer carbon inventory, both to understand natural variability at different locations, and to identify changes over time.

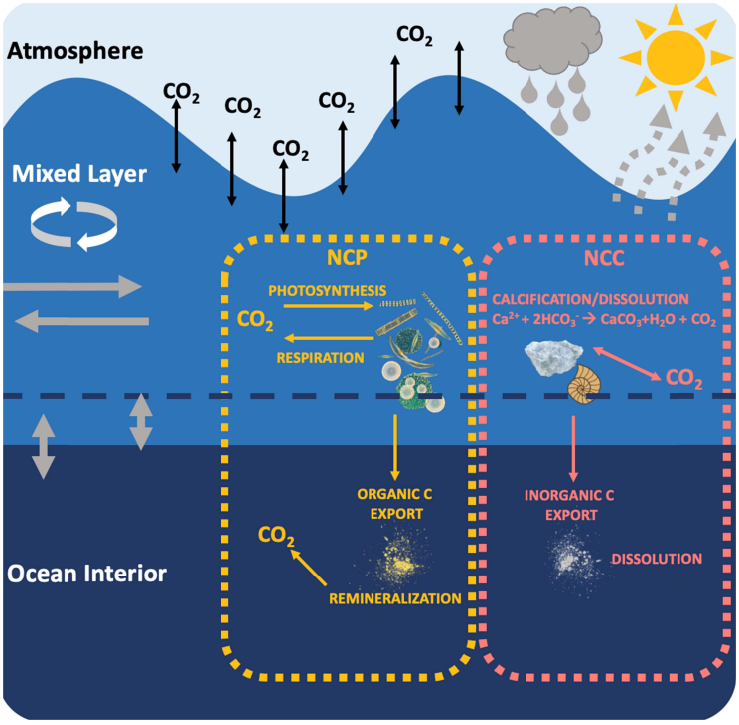

Figure 1. Schematic of processes driving mixed layer carbon cycling. Processes influencing the organic component/net community production (photosynthesis and respiration, yellow) and inorganic component/calcification (calcification and dissolution, pink) of the biological carbon pump, as well as physical processes (gas exchange, black arrows; evaporation and precipitation, advection, entrainment/detrainment, diffusion, grey arrows).

The North Pacific Subtropical Gyre (NPSG) is an essential system to study when looking at global carbon cycling. Spanning an area of 2×10^7 km^2, the NPSG is the largest ecosystem on earth, and a substantial sink for atmospheric CO_2 (Emerson, 2014). Through the Hawai‘i Ocean Time-series (HOT) at Station ALOHA (A Long-term Oligotrophic Habitat

Assessment), one of the longest running oceanic time-series at >30 years, the considerable complexity of this oligotrophic "ocean desert" has been and continues to be investigated, with a focus on biogeochemical cycling of carbon and nutrients, from various angles. Identifying and quantifying the processes at work in the subtropical oligotrophic gyres is difficult due to the very low signal-to-noise ratio in inorganic carbon and associated parameters, and the episodic nature and patchiness of biological variability (Church et al., 2013). Well-constrained community production and calcification would provide an important puzzle piece for understanding current and future ocean regimes in this important ecosystem.

Using total alkalinity (TA) and dissolved inorganic carbon (DIC) as tracers, a mass balance of mixed layer carbon production is constructed at Station ALOHA. Both the organic (Net Community Production, NCP) and inorganic (Net Community Calcification, NCC) components of the biological pump are quantified based on the differing stoichiometry of the reactions of interest (Fassbender et al., 2016, 2017). This allows the evaluation of seasonal and interannual variability in drivers of carbon cycling in the NPSG. Thanks to the abundance of complementary and redundant datasets at this well-studied location, multiple approaches to quantify several of the mass balance terms can be evaluated for consistency. Sensitivity analyses of physical transport terms, evaporation and precipitation, and mixed layer definition can illuminate the limitations of an upper ocean carbon budget at this location with present data resolution in space and time.

1.2 Study area: Station ALOHA

Station ALOHA is a time-series study site with a sampling radius of 9.66 km (6 nm) at 22°45'N, 158°W in the NPSG, 100km north of O'ahu, Hawai'i. Since 1988, approximately monthly cruises to Station ALOHA have been executed by the Hawai'i Ocean Time-series (HOT) program, capturing a variety of oceanographic parameters including thermohaline structure, water column chemistry, primary production, plankton community structure, particle export, and currents throughout the water column. In addition, since 2004, moorings within Station ALOHA (2004-2007: MOSEAN Hale-Aloha [www.pmel.noaa.gov/co2/story/HALE-ALOHA] and since 2007: WHOTS [www.soest.hawaii.edu/whots/;

www.pmel.noaa.gov/co2/story/WHOTS)]) have been recording higher-frequency variability of atmospheric and surface ocean pCO_2 (3-hourly), meteorological data, surface and sub-surface currents (from an Acoustic Doppler current profiler (ADCP) and vector measuring current meters (VMCM, Weller & Davis (1980)), and temperature and salinity in the upper 155 m (from conductivity, temperature, depth sensors (CTDs)). The unique combination and extent of observations at this site have enabled multiple ground-breaking discoveries in oceanography, such as the ubiquity of marine archaea, and also including the identification of important patterns influencing carbon biogeochemical cycling (Karl & Church, 2018). The Hawai'i Ocean Time-series is one of the places where the decrease in surface ocean pH due to anthropogenic CO_2 emissions was first clearly documented. Many researchers have conducted studies on the carbon cycle at Station ALOHA, mainly in the 1990s and early 2000s (e.g., Dore et al., 2003, 2009; Keeling et al., 2004; Brix et al., 2004, 2006; Quay & Stutsman, 2003; Neuer et al., 2002; Letelier et al., 2000; Karl et al., 1996; Winn et al., 1994, 1998). These studies on biology, physics, and especially the CO_2-carbonate system, carbon cycling, and biological production at this location provide the groundwork for this study.

1.3 The ecosystem and carbon cycle at Station ALOHA

The ocean in the NPSG is persistently oligotrophic throughout the year with a warm, nutrient-depleted surface layer that is largely isolated from the nutrient-rich deeper waters year-round. Seasons referred to here are defined as spring (March-May), summer (June-August), fall (September-November) and winter (December-February). Most biogeochemical parameters show little seasonality compared to both more temperate environments and other modes of variability (e.g., Karl & Church, 2017; Church et al., 2013). The sea surface temperature only varies by about 4-5°C seasonally (e.g., Brix et al., 2004). The mixed layer is relatively shallow year-round, between 20-120 m (Karl & Lukas, 1996), and the average mixed layer depth changes between ≈ 30-40 m in the summer-fall and ≈ 70-90 m in the winter. An important component of seasonal variability is the presence of cyclones and associated cold fronts in the winter, which result in strong winds and temporary deepening of the mixed layer (Karl, 1999). The mixed layer only reaches the top of the deep nutricline in late winter to early spring (Ascani et al., 2013). Due to minimal nutrient input, a microbial regeneration loop prevails, where nutrients are largely recycled within the surface layer (Brix et al., 2006). Nitrogen fixation is most variable during the late summer, and generally supplies around 27-45% of particulate nitrogen export (Böttjer et al., 2017). Larger particle export pulses between July-August are supported by diatom-diazotroph assemblages (DDAs), driven by a competitive transition from DDAs in the early summer to other diazotrophs (Follett et al., 2018).

Part of the declared goals of the Hawaii Ocean Time-series are to explore "*1) The linkages between seasonal, interannual and long-term (...) variability and trends in ocean physics, chemistry, and biology. 2) Processes underlying physical and biogeochemical temporal variability. 3) The role of physical forcing on carbon fluxes, including rates of biologically mediated carbon transformations, air-sea CO_2 exchange, and carbon export.*" (Church et al., 2013). A great deal of effort has already gone into research projects tackling these relationships, but many questions remain unanswered. For example, there is a disagreement in values of NCP from *in situ* compared to *in vitro* methodologies, discussed in detail by Duarte et al. (2013), Ducklow & Doney (2013), and Williams et al. (2013). Additionally, discrepancies between satellite estimates and sediment trap data, which both underestimate NCP compared to mass balance calculations such as the present budget, have been established and addressed, for example, by Emerson (2014). One of the main difficulties in resolving annual net community production and carbon export with upper ocean mass balance calculations has been the inability to fully constrain relevant lateral and vertical transport terms (Keeling et al., 2004; Dore et al., 2003). To complement previous estimates of NCP from other authors using various methodologies, this study aims to independently constrain all physical transport components, thanks to available high temporal resolution data from the WHOTS mooring, as well as horizontal gradient climatologies from neural networks (Sutton et al., 2014, Broullón et al., 2019, 2020). Additionally, a seasonal view of net community calcification is provided for the first time at this location.

2 Data and Methods

2.1 Budget components

This carbon budget quantifies a seasonal climatology from a time-dependent monthly mass balance of carbon (DIC and TA in μmol kg^{-1}), integrated over the mixed layer. It is based on a methodology developed by Fassbender and colleagues (Fassbender et al., 2016, 2017). DIC and TA are used as dual tracers.

$$\frac{\partial DIC}{\partial t} = \frac{\partial DIC}{\partial t}\Big|_{GasEx} + \frac{\partial DIC}{\partial t}\Big|_{Phys} + \frac{\partial DIC}{\partial t}\Big|_{Evap,Precip} + \frac{\partial DIC}{\partial t}\Big|_{Bio} \quad (1)$$

$$\frac{\partial TA}{\partial t} = \frac{\partial TA}{\partial t}\Big|_{Phys} + \frac{\partial TA}{\partial t}\Big|_{Evap,Precip} + \frac{\partial TA}{\partial t}\Big|_{Bio} \quad (2)$$

The observed changes in DIC and TA can be decomposed into individual process components that are calculated independently: physical transport, evaporation and precipitation, and, for DIC, gas exchange (Equations 1-2). With all of the process components and the observed change constrained, the change due to biological processes is determined from the residual. To examine the seasonal changes, monthly averages are used for each term. Monthly averages of the variables are computed for months with >20% data coverage. The physical components of change in DIC and TA over time (gas exchange, evaporation and precipitation (via concentration and dilution of carbon species), horizontal and vertical physical transport) are then evaluated and integrated over the mixed layer.

Finally, the biological term is separated into organic (NCP) and inorganic (NCC) components of biological carbon production, based on stoichiometric ratios from Anderson & Sarmiento (1994). Because organic matter- and calcium carbonate production have different effects on DIC vs. TA, we have four equations and four unknowns and can rearrange to explicitly solve for the changes due to NCP and NCC (Equations 3-6). A derivation of these equations can be found in the Supplemental Information of Fassbender et al. (2017). Many of the inputs required for the budget terms are only available as seasonal climatologies, so the results represent average annual cycles. For individual terms, several different methods were tested to evaluate consistency. These approaches are listed in Table 1, and described in detail in the respective sections and the Supplemental Information. Method A in Table 1 is the preferred methodology.

$$\frac{\partial DIC}{\partial t}\Big|_{NCP} = \frac{\left(\frac{\partial TA}{\partial t}\Big|_{Bio} - 2 \times \frac{\partial DIC}{\partial t}\Big|_{Bio}\right)}{\left(-2 + \frac{-17}{117}\right)} \quad (3)$$

$$\left.\frac{\partial \mathrm{DIC}}{\partial \mathrm{t}}\right|_{\mathrm{NCC}} = \frac{\left.\frac{\partial \mathrm{TA}}{\partial \mathrm{t}}\right|_{\mathrm{Bio}} - \left(\frac{-17}{117}\right) \times \left.\frac{\partial \mathrm{DIC}}{\partial \mathrm{t}}\right|_{\mathrm{NCP}}}{2} \quad (4)$$

$$\left.\frac{\partial \mathrm{TA}}{\partial \mathrm{t}}\right|_{\mathrm{NCC}} = 2 \times \left.\frac{\partial \mathrm{DIC}}{\partial \mathrm{t}}\right|_{\mathrm{NCC}} \quad (5)$$

$$\left.\frac{\partial \mathrm{TA}}{\partial \mathrm{t}}\right|_{\mathrm{NCP}} = \left(\frac{-17}{117}\right) \times \left.\frac{\partial \mathrm{DIC}}{\partial \mathrm{t}}\right|_{\mathrm{NCP}} \quad (6)$$

Term	**Method A**	**Alternative approaches/Sensitivity tests**	
Physical Transport: Lateral advection	**Average current, seasonal gradient fit + lateral eddy flux**	WHOTS current climatology, gradient climatology + no eddy flux	Average current, gradient climatology + lateral eddy flux
Physical Transport: Eddy Diffusivity	**Density gradient**	Heat budget	
Evaporation–Precipitation	**Salinity budget**	Meteorological sensors	Salinity normalization
Mixed Layer Depth	**T offset (–0.5°C)**	Density offsets (+0.03 kg m^3, +0.125 kg m^3)	T offset (–1°C)

Table 1. Summary of preferred methodology used for the carbon budget (Method A) and alternative approaches for sensitivity tests of individual terms.

2.2 Total alkalinity and dissolved inorganic carbon

The high temporal resolution time-series from the WHOTS mooring sensors between 2004-2019 is of two carbonate system parameters, seawater pCO_2 (pCO_2sw) and pH. However, because the seawater pH record has significant data gaps and pH is not an ideal parameter to pair with pCO_2sw to calculate DIC and TA, we use an alternative approach (McLaughlin et al., 2015; Sutton et al., 2016). To approximate DIC and TA concentrations at the same temporal resolution, two steps are necessary. First, a regression of salinity and alkalinity from HOT cruise surface data, collected at near-monthly frequency, yields a linear regional salinity-alkalinity relationship. This relationship is then applied to the WHOTS mooring surface salinity time series, which results in a high-resolution alkalinity time-series. From measured pCO_2sw and calculated alkalinity, all CO_2 carbonate system parameters, including DIC, are calculated with the CO2SYS Python package "PyCO2SYS", an adaptation from the

MATLAB version (pyco2sys.readthedocs.io; Humphreys et al., 2022a, b). Constants used are Sulpis et al. (2020) for carbonic acid and bicarbonate dissociation constants (K_1 and K_2), and Dickson (1990) for K_{SO4}. All other values used are the default terms in the PyCO2SYS package (i.e., default 0 for nutrient concentrations, K_{HF} from Dickson & Riley (1979), and the boron-chlorinity ratio from Uppström (1974)).

2.3 Mixed layer depth

Mixed layer depth (MLD) is calculated using a criterion based on a –0.5 °C change in temperature relative to the temperature at a 10-m reference depth (Sprintall & Tomczak, 1992). This criterion is one of many that is commonly used at Station ALOHA (e.g., Brix et al., 2004; Keeling et al., 2004). MLD is calculated from the daily average of temperature profiles measured by WHOTS mooring CTD sensors (sampling every minute at 5-10 m spacing), interpolated to a one-meter grid. To match the temporal resolution of the budget calculation, the monthly mean of the daily values is used. Visual inspection of all HOT TA and DIC profiles used for the analysis indicated that the –0.5 °C temperature threshold most appropriately captures *in situ* carbon system dynamics compared to other commonly used criteria (see Figure S1, Movies S1-2 for profiles and MLD). To test for sensitivity of the analysis to MLD definition, a comparison was made to three other MLD definitions: a -1°C temperature threshold (Hastenrath & Merle, 1987), as well as +0.03 kg m^{-3} and +0.125 kg m^{-3} density thresholds (De Boyer Montégut et al., 2004; Levitus, 1982), all relative to a 10-m reference depth.

2.4 Gas exchange

The contribution of gas exchange to monthly DIC change is calculated using wind speed, SST, salinity, pCO_2air and salinity-normalized pCO_2sw data all from WHOTS mooring sensors (Wind speed: http://uop.whoi.edu/currentprojects/WHOTS/whotsarchive.html, CTD: ftp://mananui.soest.hawaii.edu/pub/hot/whots/, pCO_2: Sabine et al., 2012; Sutton et al., 2012), as well as empirical relationships:

$$\left.\frac{\partial DIC}{\partial t}\right|_{GasExchange} = k \times K_H \times \Delta pCO_2 \quad (7)$$

231 Where k is the piston velocity based on wind speeds at 10m above the surface (Liu et al.,
232 1979), Schmidt number (Wanninkhof, 1992), and a second-order gas transfer
233 parameterization (Ho et al., 2006), and K_H is the CO_2 solubility constant (Weiss, 1974).
234 Details on this calculation are listed in the Supplemental Information. All measurements are
235 averaged hourly, except for the pCO_2sw and pCO_2air data, which is interpolated linearly to
236 hourly data from measurements taken every three hours. Gas exchange is evaluated hourly
237 and then averaged monthly.

238 2.5 Physical transport

239 The physical transport term described for DIC in Equation 8, and exactly the same for TA,
240 comprises horizontal transport, vertical entrainment and diffusion (adapted from Fassbender
241 et al., 2016, 2017). Individual terms and their units are listed below and in Table 2.

(8)
$$\left.\frac{\partial DIC}{\partial t}\right|_{Phys} = \left.\frac{\partial DIC}{\partial t}\right|_{Lateral\ transport} + \left.\frac{\partial DIC}{\partial t}\right|_{Entrainment} + \left.\frac{\partial DIC}{\partial t}\right|_{Diffusion}$$

Symbol	Quantity	Calculation/Source	Units
$\mathbf{u}_{ML}$	Average mixed layer current speed	WHOTS mooring sensors. Mean value from monthly averages over the complete WHOTS time-series.	m/s
κ_{HOR}	Lateral eddy diffusivity	Zhurbas & Oh (2004).	m^2/s
∇DIC	Horizontal DIC/TA gradient climatologies	Neural networks from World Ocean Atlas climatologies. Broullón et al. (2019), Broullón et al. (2020)	µmol/kg/m
w_{-h}	Vertical velocity at the ML base	Ekman pumping velocity from ASCAT wind stress curl	m/s
κ_Z	Eddy diffusivity	Climatology based on density gradients at the base of the mixed layer. Keeling et al. (2004)	m^2/s

Table 2. Terms and their units for the physical transport component of the carbon budget.

2.5.1 Lateral transport

The complete lateral transport term is calculated as the sum of horizontal background advection, and lateral eddy transport: $\boldsymbol{u}_{ML} \cdot \nabla DIC + \kappa_{HOR} \nabla^2 DIC$. For background advection, current speeds ($\boldsymbol{u}_{ML}$) and horizontal gradients in DIC and TA (∇DIC) are required, while the lateral eddy transport is quantified as a lateral eddy diffusivity (κ_{HOR}) times the Laplacian of DIC and TA fields ($\nabla^2 DIC$).

Horizontal fields of TA and DIC have been quantified elsewhere using multiple linear regression (e.g., Fassbender et al., 2016, 2017) or neural network analysis (e.g., Bittig et al., 2018; Carter et al., 2018). Climatologies around Station ALOHA from a neural network are available for both DIC (Broullón et al., 2020) and TA fields (Broullón et al., 2019). These networks networks, trained on the GLODAPv2 dataset and then applied to World Ocean Atlas (WOA) 2013 climatological data, were tested with Station ALOHA data and proved reliable for predicting TA and DIC in this region. They are used here to calculate horizontal gradients and the Laplacian of TA and DIC fields.

Advection was calculated using the overall mean WHOTS velocity in the mixed layer, and the mean plus the annual harmonic fit to the DIC and TA gradients from the Broullón et al. (2019, 2020) climatologies. In situ (WHOTS mooring) current speed measurements are available at high temporal resolution, but horizontal current speeds at this location are dominated by mesoscale eddies (Moreno et al., 2022, Figure 3a), which are not resolved by the large-scale (1°x1°) and long-term seasonal mean TA and DIC fields. An investigation into current speed variability revealed that there is no clear annual cycle (see Figure S3.2). Therefore, the overall mean current speeds with gradient climatologies best represent the advective component of this budget. The mean zonal component of the current is westward (-0.04 m s^{-1}), and the average meridional current is northward, but barely indistinguishable from zero at 0.008 m s^{-1}. This is consistent with well-established knowledge of large-scale circulation patterns at this location.

In order not to neglect the important contribution of mesoscale eddies (see e.g., Barone et al., 2019), a lateral eddy transport term is added to quantify the influence of the advective component of mesoscale eddies on the tracer budget. An average lateral eddy diffusivity from Zhurbas & Oh, (2004) of 8 x 10^3 is multiplied by the average divergence of the horizontal gradient field from Broullón et al. (2019, 2020), interpolated to a 2° latitude x 15° longitude grid to reduce noise. For the eddy contribution, a single average value is used throughout the whole year, while the advective term is at a climatological monthly resolution based on overall (non-varying) average current speed and an annual harmonic fit of monthly gradient values. An error of 100% is assigned to the lateral eddy transport.

2.5.2 Entrainment and diffusion

The entrainment term is the flux through the base of the mixed layer, primarily during times of local mixed-layer deepening. The relevant upward vertical velocity component is estimated as monthly mean Ekman pumping from Advanced Scatterometer (ASCAT)

daily wind stress curl data (from APDRC: http://www.apdrc.soest.hawaii.edu/) plus changes in mixed layer depth over time (neglecting horizontal advection of the mixed layer gradient). This term is only evaluated for periods of net entrainment; during detrainment, the properties of the water remaining in the mixed layer are not affected by the properties immediately below. Using the sum of these two terms (upward velocity and change over time in MLD), entrainment is then calculated from consecutive HOT cruise profiles in subsequent months and scaled to a monthly value, assuming that the increment of water below the first MLD is mixed into the ML by the time of the following profile. A total of 4 HOT cruise profiles (2%) were excluded due to a mismatch between MLD values and water column DIC/TA data.

As for vertical diffusive transport, vertical gradients ($\partial DIC/\partial z$) are calculated from HOT cruise profiles (again, at near-monthly resolution). The diffusion coefficient or eddy diffusivity (K_z), which governs turbulent diffusion across the bottom of the mixed layer, is not very well constrained due to considerable temporal and spatial variability, and lack of well resolved measurements (Cronin et al., 2015). It is established that turbulent diffusion is orders of magnitude higher in the surface mixed layer than in the thermocline below (e.g., Fernández-Castro et al., 2014). Previous budget or mass-balance based studies of carbon export at this location often used non-varying, representative K_z values (Table S1). However, diffusivity has been shown to vary substantially between seasons (e.g. Cronin et al., 2015). Here, we use a climatology from Keeling et al. (2004) that was calculated from measurements of the vertical density gradient just below the mixed layer.

The entrainment term is a composite of true monthly averages and near-monthly profiles, while the diffusive term and the lateral eddy transport term are based on climatological values, and hence do not resolve interannual variability. Physical transport contributions can therefore only be evaluated seasonally.

Methods for the sensitivity analysis using alternative approaches (Table 1) for the physical transport term are detailed in the Supplemental Information and include using time-varying current speed climatologies from *in situ* sensors for lateral advection, as well as a heat budget calculation adapted from Cronin et al. (2015) for diffusive transport.

2.6 Evaporation – precipitation

Adapted from Fassbender et al. (2016, 2017), E–P is determined as the residual of a mixed layer salinity budget (as in equation 8), and then scaled to units of μmol kg^{-1} according to equations 9-10. Additionally, evaporation (E) and precipitation (P) are calculated using two other approaches, to evaluate their consistency and sensitivities: A direct E-P calculation from meteorological sensors, and salinity normalization are described in the Supplemental Information.

$$\left.\frac{\partial Sal}{\partial t}\right|_{E-P} = \frac{\partial Sal}{\partial t} - \left.\frac{\partial Sal}{\partial t}\right|_{Phys} \quad (9)$$

$$\left.\frac{\partial DIC}{\partial t}\right|_{E-P} = \left.\frac{\partial Sal}{\partial t}\right|_{E-P} \times \left.\frac{DIC}{Sal}\right|_{t=0} \quad (10)$$

2.7 Error analysis

The error of the linear alkalinity-salinity fit is estimated as the standard error of the estimate (equation 11). The uncertainty of high-resolution DIC is evaluated using the error propagation tool of CO2SYS (Orr et al., 2018). Assigned uncertainties – the SE of calculated TA, as well as measurement errors for remaining parameters – are reported in Table 3.

$$SE = \sqrt{\frac{\sum(TA_{meas} + TA_{calc})^2}{N-2}} \quad (11)$$

Quantity	Error	Source
Total Alkalinity	4.95 µmol kg^{-1}	Standard Error
DIC	7.7 µmol kg^{-1}	CO2SYS error propagation (Orr et al., 2018)
Temperature	0.002 °C	Reported by manufacturer (Sea-Bird Scientific)
Salinity	0.012	Mandujano et al. (2016)
pCO_2sw	2 µatm	Sutton et al. (2014)
pCO_2air	1 µatm	Sutton et al. (2014)
MLD (h)	2.4 m	¼ of vertical separation of sensors (Fassbender et al., 2016)
Piston velocity (k)	30%	Nightingale et al. (2000), Fassbender et al. (2016)
Wind speed	0.1 m/s	https://journals.ametsoc.org/view/journals/atot/37/4/jtech-d-19-0132.1.xml
Carbon quotient in Redfield ratio	14	Anderson & Sarmiento (1994)
Turbulent eddy Diffusivity (Kz)	2.2 x 10^{-5}	Standard deviation of climatological means
Lateral eddy transport	100%	Assigned since there are no uncertainties reported for K_{LAT}

Mean mixed layer current speeds ($\mathbf{u}_{ML}$)	0.008 m s^{-1}	SEM (from autocorrelation analysis)

Table 3. Error estimates for Monte Carlo analysis and their sources.

3 Results

3.1 Surface DIC and TA time-series

A regression of total alkalinity and salinity in the top 30m provided a well-constrained relationship between the two parameters (R^2 = 0.89, n = 630), and a standard error of the estimate of 4.95 µmol kg^{-1}, (Equation 12). The propagated error (standard error propagation in CO2SYS) in DIC, calculated from this estimated TA and measured pCO_2sw is 7.7 µmol kg^{-1}. There is good agreement between HOT discrete observations of both TA and DIC with the calculated time-series of these parameters, with mean residuals of 4.0 µmol kg^{-1} for TA (discrete > calculated) and -1.7 µmol kg^{-1} for DIC (discrete < calculated), which fall within the uncertainty estimates (see Figure 2).

$$TA = 66.68 * S - 29.73 \quad (12)$$

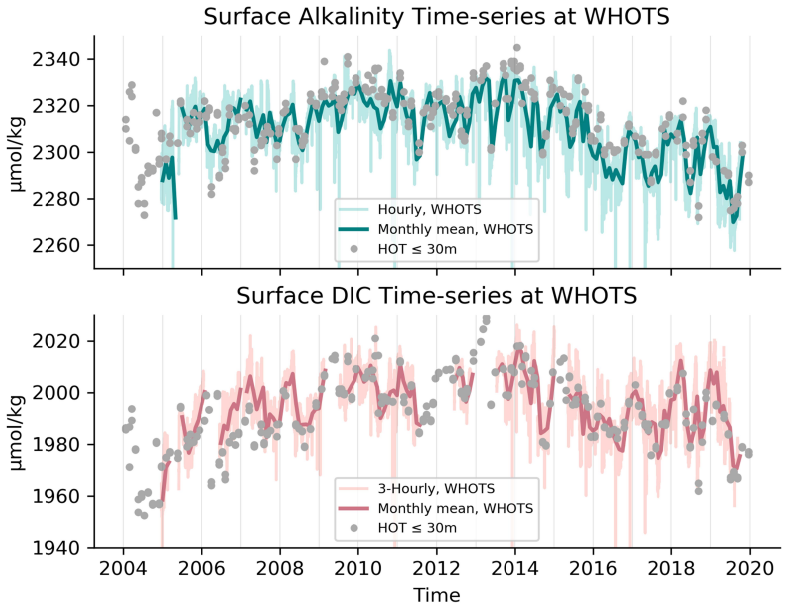

Figure 2. Surface alkalinity and DIC time-series at the WHOTS mooring, comparing upper 30m discrete HOT samples with monthly means from calculated high-resolution (3-hourly) mooring-based data.

3.2 Gas exchange

Since the whole gas exchange term is resolved at hourly frequency, we can calculate true monthly averages of this term, enabling evaluation not just of a seasonal climatology, but of changes from monthly to interannual time scales. High confidence in the monthly mean

values is confirmed by the small variance between Monte Carlo runs (see uncertainty in Table 3).

Gas exchange contributes relatively little to mixed layer DIC variability, with maxima for individual months of +3 and -4 µmol kg^{-1} mo^{-1} (corresponding to a climatological maximum CO_2 flux of +3.7 mmol m^{-2} d^{-1} for March, and a minimum of –1.8 mmol m^{-2} d^{-1} in September) (Figure 3a). The seasonal cycle is distinctive, with increasing DIC through Dec-May (uptake) and decreasing DIC in Jul-Oct (outgassing) (Figure 3a), confirming previous studies on time periods of source and sink behavior over the year (e.g., Sutton et al., 2017). Cumulative DIC change due to gas exchange is positive for each complete deployment year (June to June). An exception is the strong El Niño year 2015-2016, where an intense outgassing period in August and September 2015 yields a 2015-2016 DIC change from gas exchange that is virtually indistinguishable from zero. The average net annual uptake is 0.37 mol C m^{-2} from gas exchange at this location (Figure 3b)).

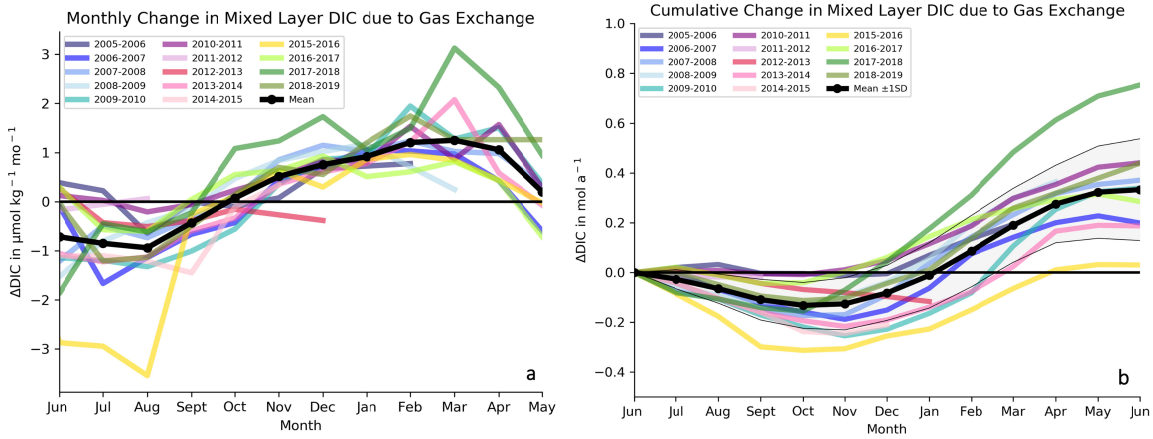

Figure 3. Change in mixed layer DIC due to gas exchange, both monthly averages in concentration change (3a), and total cumulative inputs over a year in mol C (3b).

3.3 Evaporation – precipitation

The average E–P is close to zero over a year for both DIC and TA, with net evaporation between June-October (except for August) and oscillating positive and negative values for the rest of the year (see Figure S4).

3.4 Physical transport

The physical transport term cannot be evaluated for interannual variability, as the lateral eddy flux divergence is approximated as a constant and the diffusive flux is based on a vertical eddy diffusivity (K_z) seasonal climatology. DIC changes from physical transport are positive, averaging about 2.5 µmol kg^{-1} per month with a maximum of just under 5 µmol kg^{-1} in December, and a minimum of ~1 µmol kg^{-1} in March (Figure 4a). Vertical diffusion supplies small positive inputs throughout the year, and there is a distinctive ~2 µmol kg^{-1} entrainment signal between October-December. There is a seasonal pattern in non-eddy horizontal transport, with removal of DIC throughout most of the year, as low-DIC waters are advected from the East (and, to a much smaller extent, from the South), except from

September-December where fluxes are slightly positive with high-DIC waters advected from the East. The largest contribution in addition to the entrainment signal is the yearly average lateral DIC flux divergence from mesoscale eddies, which is about 2 µmol kg^{-1} mo^{-1}, mainly due to the meridional component of flux divergence. The physical transport term for TA is similar to that of DIC, but smaller (mean: <1 µmol kg^{-1} mo^{-1}, maximum: 2 µmol kg^{-1} mo^{-1} in December), due to both a smaller entrainment peak and a smaller lateral eddy transport term (~1 µmol kg^{-1} mo^{-1}). Throughout the first half of the year, stronger TA losses from the non-eddy horizontal transport term in conjunction with smaller positive fluxes from the other terms yield overall (small) negative or near-zero values (Figure 4b).

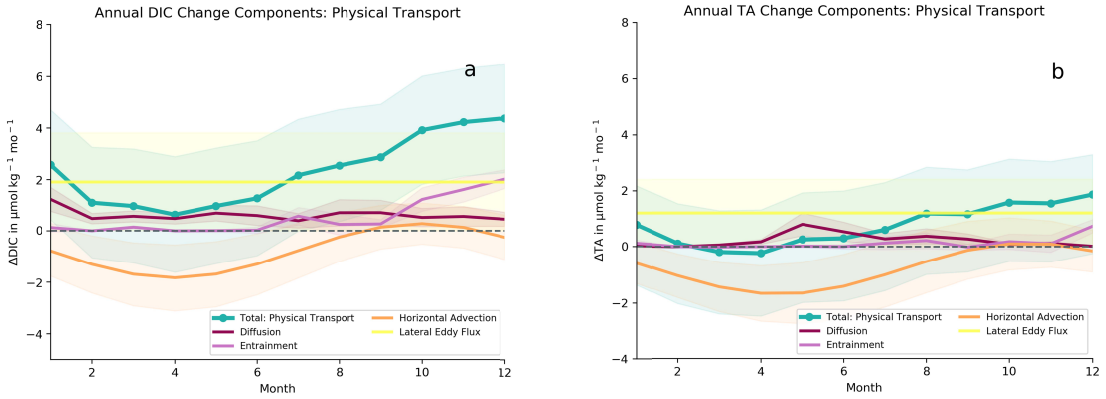

Figure 4. Yearly climatology of the physical transport term and its components for DIC (4a) and TA (4b). Shaded areas correspond to ± 1 standard deviation of Monte Carlo runs.

3.5 Biological term

The seasonal cycle of all budget terms and the observed change are shown in Figure 5. The residual contains all biological processes, as well as the errors of all other terms and any processes that are unaccounted for. The residual term for Method A closely matches the observed seasonal DIC cycle (Figure 5a), while the observed TA largely tracks the E–P term (Figure 5b), stressing the importance of concentration/dilution for TA and of biological processes for DIC over an annual cycle. The strong DIC drawdown from biological productivity and excess precipitation in the spring is balanced by DIC supply from physical transport and ingassing. A secondary peak in drawdown in the later summer is also opposed by a larger positive physical transport input, as well as additional excess evaporation, but accentuated by outgassing during the same period. Most of the observed TA seasonal cycle is explained by the E–P term, leaving a biological TA drawdown to compensate for the largely positive inputs from physical transport over a year.

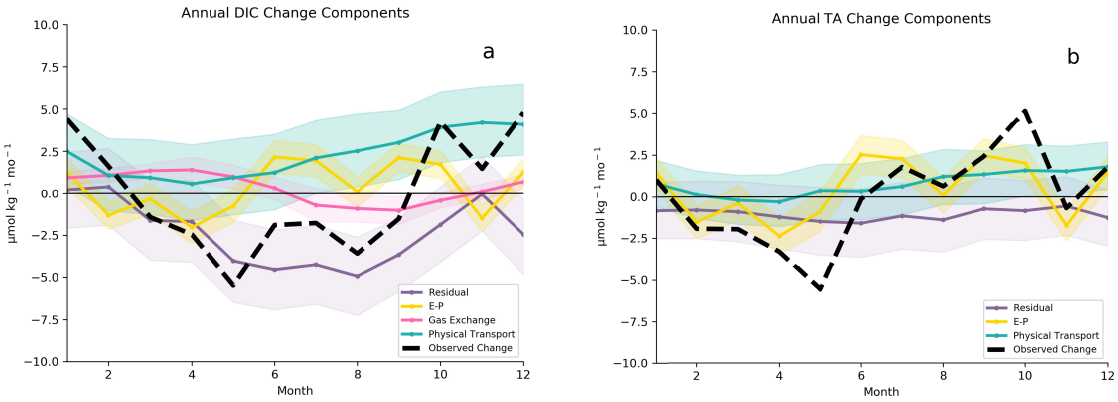

Figure 5. Yearly climatology of the biological term (residual of the budget) and model input terms for DIC (5a) and TA (5b). Shaded areas correspond to ± 1 standard deviation of Monte Carlo runs.

3.6 NCP and NCC

Figure 6 displays the seasonal cycle in NCP and NCC contributions to DIC and TA change, the two processes that compose the biological term.

The ocean at Station ALOHA is net autotrophic over the annual mean, with NCP close to zero between October and February, and relatively consistent net autotrophy (DIC loss) of about 7 mmol mo^{-1} between March and September, as well as in January (Figure 6a). The cumulative average DIC (aNCP) loss from NCP is 1.5 mol m^{-2} (Figure 6c).

TA drawdown from net calcification largely occurs in the winter and spring, between December and April, with values close to zero in the remaining months yielding net calcification (TA loss) over a year (Figure 6b). Cumulative NCC (aNCC) was 0.6 mol m^{-2} of TA drawdown (Figure 6d).

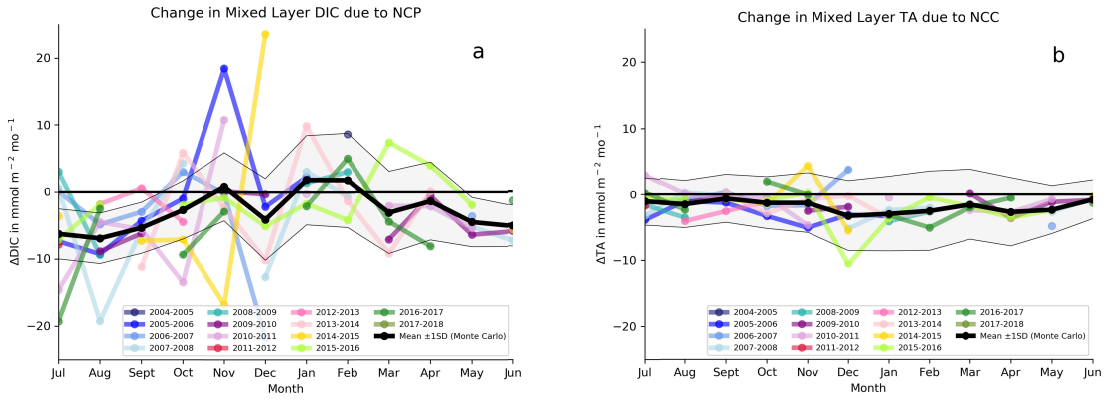

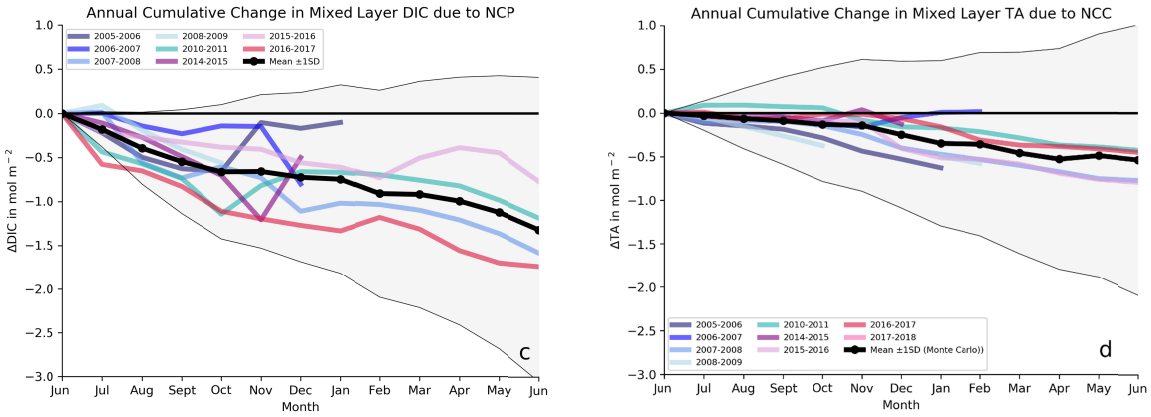

Figure 6. Yearly climatology of mixed layer NCP and NCC rates (6a,b), and (cumulative) aNCP and aNCC (6c, d), as well as averages for each year. Shaded area represents ± 1 standard deviation of Monte Carlo runs. Only complete years shown for 6c, d.

4 Discussion

4.1 Discrepancies and sensitivity tests

Study	**Method**	**Time**	**Depth**	**aNCP** (- mol C m^{-2} yr^{-1})	**(mean) NCP rate** (- mmol C m^{-2} d^{-1})
Emerson et al. (2008)[a]	O_2/Ar budget	2004 –2005	ML	-4.2 ± 1.9	-11.5 ± 5.2
Keeling et al. (2004)	Diagnostic box model (DIC & $\delta^{13}C$)	1988 –2002	ML	-2.2 ± 0.8	-6.0 ± 2.2
Lee (2001)[a]	DIC change	Summer 1990	ML	-2.3 ± 0.8	-6.3 ± 2.2
Quay et al. (2009)[a]	Carbon budget (DIC & $\delta^{13}C$)	2004 –2005	ML	-2.4 ± 1.0	-7.85 ± 2.19
Quay et al. (2010)[a]	O_2/Ar budget	2006 –2007	ML	-3.7 ± 1.0	-10.1 ± 2.7
Quay & Stutsmann (2003)	Carbon budget (DIC & $\delta^{13}C$)	1994 –1999	ML	-2.3 ± 1.3	-6.3 ± 3.4
Wilson et al. (2015)	Prior O_2/Ar-NCP	Jul-12	ML	-	-6.0 ± 3.2
Wilson et al. (2015)	Prior O_2/Ar-NCP	Aug-12	ML	-	7.6 ± 4.2
Wilson et al. (2015)	Prior O_2/Ar-NCP	Aug – Sep 2012	ML	-	0.5 ± 3.1
Sonnerup et al. (2013)[a]	CFC/SF_6 model	2008	Winter ML	-2.5 ± 3.0	-6.8 ± 8.2
Yang et al. (2017)[a]	O_2 budget	2014 –2018	Winter ML	-2.4 ± 0.6	-6.6 ± 1.6
Emerson et al. (1995)[a]	O_2/Ar/N_2 budget	1990	0-100m	-1.0 ± 0.7	-2.7 ± 1.9

Emerson et al. (1997)[a]	$O_2/Ar/N_2$ budget	Early 1990s	0-100m	-2.7 ±1.7	-7.4 ± 4.7
Sonnerup et al. (1999)[a]	CFC model	1991	0-100m	-2.2 ± 0.5	-6.0 ± 1.4
Hamme & Emerson (2006)[a]	$O_2/Ar/N_2$ budget	2000 –2001	0-115m	-1.1 ± 0.5	-3.0 ± 1.4
Benitez-Nelson et al. (2001)	^{234}Th /^{238}U disequilibri-um	1999 – 2000	0-150m	-1.5 ± 0.8	-4.0 ± 2.3 (PC flux)
Brix et al. (2006)	Diagnostic box model (DIC & $\delta^{13}C$)	1989 –2000	0-150m	-3.1 ± 0.3	-8.5 ± 0.8
Ferrón et al. (2021)	O_2/Ar	2014 –2018	0-150m	-1.5 ± 0.4	-4.1 ±1.1
Riser & Johnson (2008)[a]	O_2 budget	2002 –2005	0-150m	-1.6 ± 0.2	-4.4 ± 0.5
Emerson (2014)	Average of literature values	-	-	-2.5 ± 0.7	-6.8 ± 1.9
This study	***Carbon budget (DIC & TA), Method A***	***2005 - 2019***	***ML***	***-1.5 ± 1.7***	***-3.4 ± 2.8***

Table 4. Literature comparison of average NCP rates and aNCP values at Station ALOHA. [a] – adapted from Ferrón et al., (2021).

Study	**Term**	**Value**	**Units**
Karl et al. 2021	Average HOT PIC flux 2001-2019	24.2 2.9	mg $CaCO_3$ m^{-2} d^{-1} mg C m^{-2} d^{-1}
Dong et al. 2019	$CaCO_3$ flux near ALOHA @100m depth	71.1 8.5	mg $CaCO_3$ m^{-2} d^{-1} mg C m^{-2} d^{-1}
Betser et al. 1985	Pteropod (aragonite) fluxes at 100m. 21°N, Western North Pacific	32.6	mg $CaCO_3$ m^{-2} d^{-1}
		3.9	mg C m^{-2} d^{-1}
Sabine 1995a	Carbonate flux from dissolution	40 4.8	mg $CaCO_3$ m^{-2} d^{-1} mg C m^{-2} d^{-1}
Sabine & Mackenzie 1995	Sediment trap $CaCO_3$ flux - HOT-7 200m	40.3 4.8	mg $CaCO_3$ m^{-2} d^{-1} mg C m^{-2} d^{-1}
Sabine & Mackenzie 1995	Sediment trap $CaCO_3$ flux - HOT-9 200m	40.7 4.8	mg $CaCO_3$ m^{-2} d^{-1} mg C m^{-2} d^{-1}
Sabine & Mackenzie 1995	Sediment trap $CaCO_3$ flux - HOT-11 200m	39.4 4.7	mg $CaCO_3$ m^{-2} d^{-1} mg C m^{-2} d^{-1}
Sabine & Mackenzie 1995	Sediment trap $CaCO_3$ flux - HOT-15 200m	40.8 4.9	mg $CaCO_3$ m^{-2} d^{-1} mg C m^{-2} d^{-1}
This study	**Mean mixed layer TA change from NCC**	**170** **20.4**	**mg $CaCO_3$ m^{-2} d^{-1}** **mg C m^{-2} d^{-1}**

Table 5. Literature comparison of average carbonate fluxes at Station ALOHA in different units.

Results of this study are on the lower end of the reported range for aNCP at this location (1.5 vs mean 2.0 mol m^{-2}, see Table 4.1). However, given error estimates here and in previous studies, none of the aNCP estimates are significantly different from the results presented here (see Table 4). By contrast, average aNCC is four to seven times larger than HOT sediment trap results, which constitute the only available dataset with which to compare (Table 5). Sediment traps are known to provide a lower-end estimate for PIC and PC export fluxes, but an inorganic carbon flux making up 30% of total carbon export is likely to be an overestimation at this site. A sensitivity analysis investigating different methodologies to quantify most of the terms of this carbon budget can shine a light on the origins of and insights from the divergence we see in average aNCP, and especially aNCC values compared to previous reports. The alternative methods used for E–P, horizontal transport, and diffusion terms are listed in Table 1 and expanded upon in the Supplemental Information. Figure 7 shows NCP and NCC calculated using these methods.

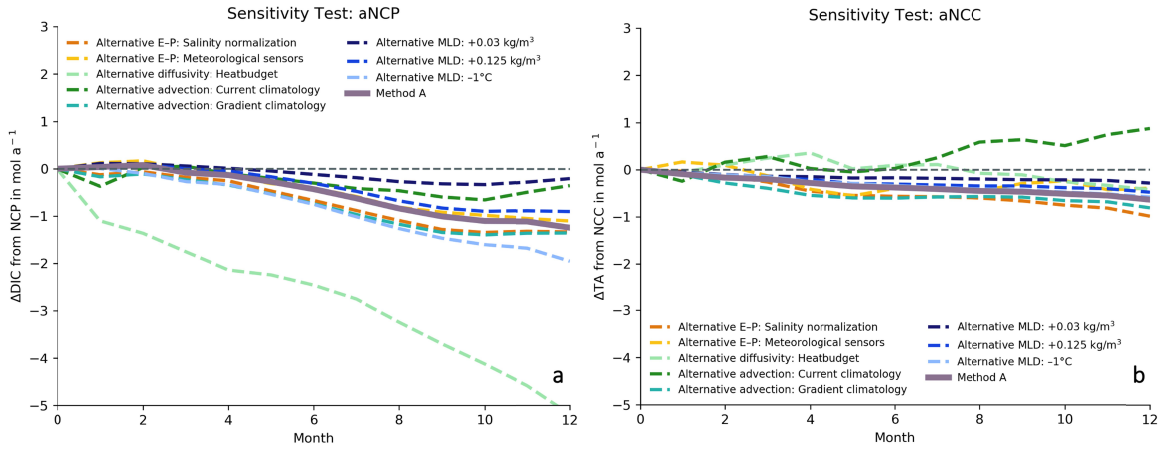

Figure 7. Sensitivity test for all different methodologies showing resulting Monte Carlo average aNCP (7a) and aNCC (7b).

4.1.1 Gas exchange

Annual CO_2 invasion here is 0.37 mol m^2. This estimate is much lower than previous estimates based on pCO_2 calculated from discrete TA and DIC measurements (e.g. Quay & Stutsman (2003): 0.6 ± 0.4 mol C m^{-2}, Dore et al. (2009): ~0.5 mol C m^{-2}), and underway pCO_2 data (Takahashi et al., 2009) but equivalent to earlier estimates from the WHOTS mooring (Sutton et al., 2017). A discrepancy between WHOTS flux estimates and underway pCO_2 systems was previously reported as 60%, and explained partly by differences in wind speed parameterization (Sutton et al. (2017)). Additionally, there is an average offset of about 8 µatm in measured pCO_2 at the WHOTS mooring compared to calculated pCO_2 from HOT measurements, which is small (2% of the mean) but grows considerably when integrated over time such as in integrated annual flux calculations. Possible contributors to this offset include differences in temperature (and therefore pCO_2) due to measuring depth (<1m for WHOTS, 5-30m for discrete data), conditions

within the mooring measurement apparatus (equilibrator) not representing mean mixed layer pCO_2, or a systematic underestimation of pCO_2 calculated from TA & DIC. For this budget, both underestimated ingassing in the spring/summer and overestimated outgassing in the fall would entail underestimated NCP rates for these same months, and could partly be responsible for the relatively low aNCP reported here. Additionally, since for this budget CO_2 invasion is converted to a concentration change and then integrated over the mixed layer, the choice in mixed layer depth definition also impacts the gas exchange term, with a shallower mixed layer accentuating both outgassing and ingassing signals (see Figure S4b).

4.1.2 Horizontal transport

The contribution of advection and diffusion to the DIC budget has been unclear in both magnitude and seasonality in previous studies (Dore et al., 2014, 2009; Keeling et al., 2004). Despite the extraordinarily abundant data from the long-standing Hawaii Ocean Time-series project, the high-resolution data needed in both time and space to accurately quantify physical transport fluxes of carbon species has not been available. Nonetheless, progress in quantifying both horizontal and vertical inputs of DIC and TA may be possible by using newer data products including the high temporal resolution WHOTS mooring current speeds and horizontal gradient climatologies from neural networks (Broullón et al., 2019, 2020).

Unfortunately, data availability for horizontal gradients and eddy diffusivity still restricts us to a *seasonal* budget. The effect of using a time-varying current speed climatology instead of average current speeds to constrain horizontal transport illustrates a basic problem with using a seasonal budget approach at this location, where seasonality explains only a small fraction of the variability. For both DIC and TA, interannual variability is much larger than the amplitude of a seasonal cycle, with a variance in monthly averages of about 30-50 μmol kg^{-1} between years, but an average seasonal cycle of only about 15 μmol kg^{-1}. As discussed in the methods section, current speeds at this location are dominated by mesoscale eddies, and also do not vary strongly with season at Station ALOHA (see Figure S3.2).

For a sensitivity check, using a current speed climatology from WHOTS ADCPs, instead of the average current speed used in Method A, drastically changes the horizontal transport term for TA and DIC (Figure S4), and consequently also NCC and NCP (Figure 7b). This is mainly based on the average direction of transport for individual months of the current climatology (Figure S2). However, this average direction does not represent any “real” seasonality in current speed and direction, as the currents have been shown to have no significant seasonality (Figure S3) – so the seasonality of the modified advective term is questionable. At locations of previous studies using this approach (Fassbender et al., 2016, 2017), horizontal contributions to the overall carbon budget were negligible or small compared to other budget components. Due to a much smaller contribution of vertical mixing and entrainment, at this location the advective term becomes the most important physical transport process (Figure 4). It is therefore likely that the discrepancy between NCP & NCC calculated here and literature values can partly be explained by the inability to meaningfully evaluate this important term on a seasonal time-scale.

This illustrates the need for data on horizontal gradients of surface carbonate chemistry parameters at higher spatiotemporal resolution, as will hopefully be achieved by promising current and future endeavors using floats, autonomous vehicles, and satellites (e.g., Nicholson et al., 2022; Nickford et al., 2022). With data on variability in TA/DIC gradients at the spatiotemporal scale of mesoscale eddies, the construction of a carbon budget at the appropriate time scale(s) would be possible, and the importance of horizontal transport for carbon cycling at this location could be investigated.

The annual cycle calculated here using Method A shows advective DIC and TA loss especially in the early spring (DIC) and summer (TA), driven by a small zonal component of the gradient, both parameters increasing to the west. Interestingly, previous studies have neglected zonal transport due to the small gradients (e.g., Dore et al., 2009, Keeling et al., 2004), and indeed meridional gradients in DIC and TA are much steeper throughout the year, with both parameters increasing northward (see Supplemental Information, Figure S3c-d). However, the weak mean meridional flow (average 0.008 m s^{-1}) contributes only a small loss, the net advective term is dominated by the stronger mean zonal flow acting on the seasonally varying zonal gradient.

4.1.3 Vertical transport

For the vertical transport term, a heat budget based on Cronin et al. (2015) was constructed to constrain eddy diffusivity in a different way (see Supplemental Information). Since there are order of magnitude differences in the climatological diffusivity values generated by the Keeling et al. (2004) and the Cronin et al. (2015) approach, a sensitivity analysis to the choice of diffusivity coefficients was performed. Generally, due to increasing DIC with depth (a positive vertical DIC gradient), higher K_z will lead to increased diffusive DIC fluxes into the mixed layer, which, in turn, propagates to a larger biological term and more DIC drawdown from NCP (essentially balancing higher K_z input values). For TA, the relationship is less straightforward due to an alkalinity maximum associated with the North Pacific Tropical Water (NPTW) at Station ALOHA that varies in location relative to the mixed layer (Lukas & Santiago-Mandujano, 2008). Both time-varying K_z estimates show a peak in diffusive transport in the spring, and the shape of the annual cycles is remarkably similar, but they differ by an order of magnitude across their whole range (Figure S5). The Keeling et al. (2004) data is more in line with literature data, and the calculation based on the heat budget yields (unrealistic) negative values indicating up-gradient transport in the fall. As Table S3 shows, the choice of K_z values strongly impacts the final NCP and NCC results, especially in the springtime when biological drawdown of DIC is most prevalent. Therefore, more measurements and refined budget calculations using float and mooring data to constrain K_z values at various temporal and spatial scales would be very useful for biogeochemical tracer budgets such as this one.

4.1.4 Evaporation – precipitation

E–P using a salinity budget (Method A) vs. salinity normalization are very similar, while the calculation based on WHOTS measurements yields much smaller fluxes (Figure S4, S5). They all converge on (maximum) net evaporation during the summer/fall, between

June and October. With the direct calculation from mooring sensors, net evaporation persists throughout the year, while the other two approaches largely indicate net precipitation earlier in the year (Feb-May). The large discrepancy between the salinity-based and the directly measured approaches can partly be explained by rainfall measurements. Mooring precipitation sensors do not match satellite, shipboard or model results, largely due to the extreme patchiness of rainfall.

However, it is also likely that unresolved advective processes affect the salinity-based calculation, but that those contributions are cancelled out in the final carbon budget. The residual of the salinity budget contains all errors and fluxes that are not accounted for in the physical transport terms. E–P is the residual of the salinity budget, and appears to be driving most of the observed salinity variations; this suggests an underestimation of physical transport terms, as local precipitation and evaporation are not expected to be the main control of sea surface salinity. We assume that any unresolved processes affecting salinity are essentially conservative mixing processes (i.e., they affect TA and DIC proportionally), such as advection of regional gradients in salinity (and TA, DIC) from local precipitation differences that are not captured by 1°x1° climatological fields. Consequently, the use of the salinity budget for the E–P term is beneficial for the final carbon mass balance. Since the (scaled) salinity physical transport term is subtracted from the DIC/TA physical transport terms, any biases that they both exhibit should cancel out, similarly as discussed in Fassbender et al. (2016, Equation 10); while this shows again that the physical transport term taken alone is likely not resolving important contributions, this increases the confidence in final NCC and NCP values.

4.1.5 Mixed-layer depth

Several definitions of mixed layer depth have been used at Station ALOHA, including the density criteria of +0.03 kg m^{-3} from De Boyer Montégut et al. (2004) (e.g. Ferrón et al., 2021; Barone et al., 2019; Karl et al., 2021), and 0.125 kg m^{-3} from Levitus (1982) (e.g., Dore et al., 2003, 2009, 2014; Quay & Stutsman, 2003; Wilson et al., 2015), as well as the temperature criterion of -1°C from Hastenrath & Merle (1982) (e.g. Venrick, 1993; Cortés et al., 2001). All MLD criteria yield very similar NCC estimates. While the general shape of the seasonal DIC changes from NCP is the same for all MLD estimates, the magnitude of these fluxes varies more between different estimates, leading to differences of cumulative aNCP from 0.25 mol m^{-2} using the +0.03 kg m^{-3} density criterion (shallower ML definition) to ~2 mol m^{-2} using a -1°C temperature threshold (deeper ML definition). Although all of these estimates are within the aNCP error, this illustrates the importance of MLD definition for mixed layer carbon budgets.

It is worth mentioning that discrepancies between multiple approaches to some of these terms could only be exposed due to the unusual abundance of various complementary and redundant datasets at Station ALOHA, and could have easily gone unnoticed in other locations with less available data. There are issues with constraining seasonal fluxes of several key contributors to the carbon budget at this location compared to other studies, but the challenges adapting this approach are interesting results themselves: At Station ALOHA, where seasonal changes in mixed layer depth and stratification are much smaller than in the temperate ocean, constraints on (horizontal) transport from mesoscale eddies at the

583 appropriate spatial resolution become a crucial ingredient for an accurate mixed layer carbon
584 budget, and depending on MLD definition, NCP can differ by about 100%. Additionally, and
585 nonetheless, valuable insights can be gained from the budget components and final
586 aNCC/aNCP estimates obtained from the most reliable (Method A) combination of
587 methodologies, including a comparison of identified drivers of the seasonal carbon cycle and
588 their relative contributions and timing to previously published studies.

589 4.2 Drivers of the seasonal carbon cycle

590 Previous studies that utilized carbon budget models at Station ALOHA either constrained
591 vertical diffusive fluxes and inferred horizontal transport (Keeling et al., 2004), or vice versa
592 (Quay & Stutsman, 2003), with results varying considerably based on these assumptions.
593 According to Keeling et al. (2004), the main processes behind mixed layer DIC variability
594 are biological productivity, gas exchange and horizontal transport, as well as a period of
595 winter entrainment. There is agreement that the largest signal is a summer drawdown of
596 (salinity normalized) DIC due to biological activity (Quay & Stutsman, 2003; Keeling et al.,
597 2004). The amplitude of this seasonal DIC drawdown is dampened, because gas exchange is
598 strongest around the same time, but acts in opposite direction: The air to sea flux is highest in
599 spring (around April), when NCP strongly decreases mixed-layer DIC (Keeling et al., 2004).
600 These observations are largely confirmed by this study, with a small difference in timing.
601 Maximum ingassing occurs in March-April, and maximum drawdown from NCP in May-
602 Aug (Figure 6a). This is consistent with a peak in primary productivity later in the spring due
603 to increased light and nutrient availability (from deepening PAR attenuation and a shoaling
604 nutricline), and potential contribution from nitrogen-fixing cyanobacteria that are known to
605 bloom with increasing stratification in the late summer (e.g., Karl & Church, 2017). The
606 main processes that dampen the spring DIC drawdown here are physical transport, as well as
607 ingassing of DIC between March-May, both at about 1-2 μmol kg^{-1} mo^{-1}. Later in the
608 summer, the continued biological DIC drawdown from NCP is enhanced by outgassing of
609 DIC, but dampened by excess evaporation and by increased physical transport inputs.

610 In a recent study on net community production at Station ALOHA from oxygen dynamics,
611 Ferrón et al. (2021) reported lower NCP rates between December and February, followed by
612 an increase through June and then mostly high values (i.e., net autotrophy) through
613 November. In this study, the NCP increase starts later, from Apr-Jun, and we observe a shift
614 to near- zero NCP by October. Ferrón et al. (2021) suggest that their NCP_{ML} values in the
615 late fall might be too high and suggest correcting for entrainment diffusive fluxes of oxygen
616 by up to 65-100% for individual months between Sep-Nov, which would lead to a 12%
617 reduction in their aNCP estimate.

618 Studies on calcium carbonate production and dissolution at Station ALOHA and in the NPSG
619 are relatively sparse. Some studies in the 1980s and 1990s (e.g., Betser et al., 1984; Sabine et
620 al., 1995; Sabine & Mackenzie, 1995). Sabine & Mackenzie (1995) reported an export of
621 around 40mg $CaCO_3$ m^{-2} d^{-1}, and interestingly first detected the presence of calcium
622 carbonate particles from benthic, more soluble calcifying organisms living on shallow, near-
623 coastal banks in the water column at this location. To our knowledge, so far there have been
624 no attempts to quantify seasonal variability in calcification/dissolution and $CaCO_3$ export
625 dynamics at Station ALOHA. Cortés et al. (2001) studied the ecology of coccolithophores, an

important calcifying phytoplankton, and found extremely low abundances throughout most of the year. Only during March and September/October, a fairly specific range of environmental conditions regarding temperature (20-25°C), salinity (34.9-35.2), nutrients (0.004-0.07µmol/kg nitrate, <0.025µmol/kg phosphate), and light availability (2-25µE m^{-2} s^{-1}) appears to enable these higher cell densities (Cortés et al., 2001). Only a very small fraction of zooplankton at Station ALOHA was reported to be made up of shelled pteropods (Steinberg et al., 2008), but they are likely a significant contributor to PIC export due to their large size. Foraminifera, calcifying zooplankton, were examined by Monteagudo (2016) using bottom-moored sediment traps, and found to be more abundant during the summer months. Boeuf et al. (2019) investigated species composition of particles retained in deep sea sediment traps, and found foraminifera to be sporadically present in large concentrations, and pteropods generally abundant in deep sea particles. The sparse information on these three most important groups of calcifying organisms illustrates the highly variable nature of PIC export at Station ALOHA for each of them, highlighting the need for more species-specific studies of these organisms and the drivers of associated export events.

5 Conclusions and outlook

This study is a first attempt to quantify seasonality in calcification/dissolution dynamics at Station ALOHA, and results show annual net calcification of 0.5 mol m^{-2}. This exceeds all previously reported fluxes from sediment trap data, with maximum export occurring during December-April.

The mixed layer ecosystem at Station ALOHA is confirmed to be net autotrophic over a year, at about 1.5 mol C m^{-2}. Biological drawdown during March-September exceeds the inputs from physical transport processes, which are positive throughout the year with a distinct fall-winter peak. Contributions to DIC changes from evaporation and precipitation and gas exchange show clear opposing seasonal cycles.

At Station ALOHA, it would be particularly beneficial to resolve more than the annual cycle of carbon parameters, as variability on other time-scales is large compared to seasonal variations. This would require, most urgently, a dataset constraining regional horizontal gradients in alkalinity and DIC at near-monthly time scales, as could potentially be developed from algorithms employing satellite data, as well as regional-scale ocean models.

Further research into the impacts of climate change on the drivers of the upper ocean carbon cycle, such changes in stratification, precipitation, and biological productivity is needed. The mixed layer carbon budget approach illustrates that a shift in timing or magnitude of the relevant processes over a year could significantly impact observed carbon chemistry, and therefore CO_2 source vs. sink behavior of the NPSG.

Acknowledgments

Thank you to Eric Firing for frequent, thorough, and thoughtful support with conceptual and practical challenges. Thanks to the crewmembers and scientists running the Hawaii Ocean Time-series over the last three decades, especially Dan Sadler for the carbonate system samples and measurements. The HOT program is supported by the National Science Foundation (current

grant OCE-1756517; AEW, P.I.). The WHOI Hawaii Ocean Timeseries Station (WHOTS) is supported by the National Oceanic and Atmospheric Administration (NOAA) Global Ocean Monitoring and Observing Program through the Cooperative Institute for the North Atlantic Region (CINAR) under Cooperative Agreement NA14OAR4320158. NOAA CPO FundRef number (100007298). Subsurface measurements are supported by NSF as part of the Hawaii Ocean Timeseries (HOT) through grants OCE-752606, 0926766, 1260164 and 1756517. We acknowledge the financial support of our research provided in part by a grant/cooperative agreement from the National Oceanic and Atmospheric Administration, CMAR award # NA21NMF4320043. The views expressed herein are those of the author(s) and do not necessarily reflect the views of NOAA or any of its subagencies. There are no perceived financial or other conflicts of interests for any author. This is SOEST contribution number ####, and PMEL contribution number 5449.

Open Research

Shipboard Hawaii Ocean Time-series bottle and CTD data is available through the HOTDOGS database at https://hahana.soest.hawaii.edu/hot/hot-dogs/interface.html. WHOTS and MOSEAN mooring pCO_2, SST and salinity data are available at https://www.nodc.noaa.gov/ocads/oceans/Moorings/WHOTS_158W_23N.html and https://www.nodc.noaa.gov/ocads/oceans/Moorings/MOSEAN.html. WHOTS subsurface CTD, ADCP and VMCM datasets can be found at ftp://mananui.soest.hawaii.edu/pub/hot/whots/, while surface meteorological data and heat flux can be accessed via http://uop.whoi.edu/currentprojects/WHOTS/whotsarchive.html, http://uop.whoi.edu/ReferenceDataSets/whotsreference.html, and http://tds0.ifremer.fr/thredds/catalog/CORIOLIS-OCEANSITES-GDAC-OBS/DATA_GRIDDED/WHOTS/catalog.html?dataset=CORIOLIS-OCEANSITES-GDAC-OBS/DATA_GRIDDED/WHOTS/. Wind stress data is available at http://apdrc.soest.hawaii.edu/erddap/griddap/hawaii_soest_a6ab_91f7_b38f.html. Satellite SST used in the heat budget can be accessed at http://apdrc.soest.hawaii.edu/thredds/dodsC/las/oisst_avhrrv20/data_apdrc.soest.hawaii.edu_dods_public_data_NOAA_SST_OISST_AVHRR_daily_v2.0.jnl.

References

Anderson, L., and Sarmiento, J. (1994). Redfield ratios of remineralization determined by nutrient data analysis. *Global Biogeochemical Cycles, 8*(1), 65–80.

Ascani, F., Richards, K. J., Firing, E., Grant, S., Johnson, K. S., Jia, Y., Lukas, R., & Karl, D. M. (2013). Physical and biological controls of nitrate concentrations in the upper subtropical North Pacific Ocean. *Deep Sea Research Part II: Topical Studies in Oceanography*, *93*, 119-134.

Barone, B., Coenen, A.R., Beckett, S. J., Mcgillicuddy, D. J. Jr., Weitz, J. S., & Karl, D.M., (2019). The ecological and biogeochemical state of the North Pacific Subtropical Gyre is linked to sea surface height. *Journal of Marine Research, 77*(2), 215-245.

Benitez-Nelson, C., Buesseler, K. O., Karl, D. M., & Andrews, J. (2001). A time-series study of

711 particulate matter export in the North Pacific Subtropical Gyre based on 234Th: 238U
712 disequilibrium. *Deep Sea Research Part I: Oceanographic Research Papers*, *48*(12), 2595-
713 2611.
714
715 Bittig, H., Steinhoff, T., Claustre, H., Fiedler, B., Williams, N., Sauzède, R., Kötzinger, A., &
716 Gattuso,
717 J., (2018). Nutrient concentrations from T, S, and O2 data using Bayesian neural
718 networks. *Frontiers in Marine Science, 5,* 328.
719
720 Böttjer, D., Dore, J.E., Karl, D.M., Letelier, R.M., Mahaffey, C., Wilson, S.T., Zehr, J., Church, M.J.,
721 (2017). Temporal variability of dinitrogen fixation and particulate nitrogen export at
722 Station ALOHA. *Limnology and Oceanography, 62*(1), 200–216.
723 https://doi. org/10.1002/lno.10386
724
725 Boeuf, D., Edwards, B. R., Eppley, J. M., Hu, S. K., Poff, K. E., Romano, A. E., Caron, D.A., Karl,
726 D.M.,
727 & DeLong, E. F. (2019). Biological composition and microbial dynamics of sinking
728 particulate organic matter at abyssal depths in the oligotrophic open ocean. *Proceedings*
729 *of the National Academy of Sciences*, *116*(24), 11824-11832.
730
731 Boyd, P.E., Claustre, H., Levy, M., Siegel, D.A., & Weber, T., (2019). Multi-faceted particle pumps
732 drive carbon sequestration in the ocean. *Nature, 568,* 327-335.
733
734 Brix, H., Gruber, N., Karl, D., & Bates, N., (2006). On the relationships between primary, net
735 community, and export production in subtropical gyres. *Deep-Sea Research II, 53,* 698-
736 717.
737
738 Brix, H., Gruber, N., & Keeling, C.D., (2004). Interannual variability of the upper ocean carbon
739 cycle at station ALOHA near Hawaii. *Global Biogeochemical Cycles, 18,* GB4019.
740
741 Broullón, D., Pérez, F., Velo, A., Hoppema, M., Olsen, A., Takahashi, T., Key, R., Tanhua, T.,
742 González-Dávila, M., Jeansson, E., Kozyr, A. & van Heuven, S., (2019). A global monthly
743 climatology of total alkalinity: A neural network approach. *Earth System Science Data,*
744 *11,* 1109-1127.
745
746 Broullón, D., Pérez, F. F., Velo, A., Hoppema, M., Olsen, A., Takahashi, T., Key, R., Tanhua, T.,
747 Santana-Casiano, J. M., & Kozyr, A. (2020). A global monthly climatology of oceanic total
748 dissolved inorganic carbon: a neural network approach. *Earth System Science Data*,
749 *12*(3), 1725-1743.
750
751 Carter, B. R., Feely, R. A., Williams, N. L., Dickson, A. G., Fong, M. B., & Takeshita, Y.
752 (2018). Updated methods for global locally interpolated estimation of alkalinity, pH, and
753 nitrate. *Limnology and Oceanography: Methods*, *16*(2), 119-131.
754

Church, M.J., Lomas, M.W., & Muller-Karger, F., (2013). Sea change: Charting the course for biogeochemical ocean time-series research in a new millennium. *Deep-Sea Research II*, 93, 2-15.

Claustré, H., Legendre, L., Boyd, P., & Levy, M. (2021). The oceans' biological carbon pumps: Framework for a research observational community approach. *Frontiers in Marine Science*, *8*, 780052.

Cortés, M.Y., Bollmann, J., & Thierstein, H.R., (2001). Coccolithophore ecology at the HOT station ALOHA, Hawaii. *Deep-Sea Research II, 48,* 1957-1981.

Cronin, M. F., Pelland, N. A., Emerson, S. R., & Crawford, W. R. (2015). Estimating diffusivity from the mixed layer heat and salt balances in the North Pacific. *Journal of Geophysical Research: Oceans*, *120*(11), 7346-7362.

De Boyer Montégut, C., Madec, G., Fischer, A.S., Lazar, A., & Iudicone, D., (2004). Mixed layer depth over the global ocean: An examination of profile data and a profile-based climatology. *Journal for Geophysical Research - Oceans 109*(C12), C12003. doi: 10.1029/2004JC002378

Denman, K. L., & Gargett, A. E. (1983). Time and space scales of vertical mixing and advection of phytoplankton in the upper ocean. *Limnology and Oceanography*, *28*(5), 801-815.

Dickson, A.G., (1990). Standard Potential of the Reaction: AgCl(s) + 1/2H2(g) = Ag(s) + HCl(aq), and the Standard Acidity Constant of the Ion HSO4- in Synthetic Seawater from 273.15 to 318.15 K. *Journal of Chemical Thermodynamics, 22*(2), 113-127. doi:10.1016/0021-9614(90)90074-Z

Dickson, A. G., and Riley, J. P. (1979). The estimation of acid dissociation constants in sea-water media from potentiometric titrations with strong base. II. The dissociation of phosphoric acid. *Marine Chemistry* 7, 101–109. doi:10.1016/0304-4203(79)90002-1.

Dong, S., Berelson, W., Rollins, N., Subhas, A., Naviaux, J., Celestian, A., Liu, X., Turaga, N., Kemnitz, N., Byrne, R., & Adkins, J., (2019). Aragonite dissolution kinetics and calcite/aragonite ratios in sinking and suspended particles in the North Pacific. *Earth and Planetary Science Letters,* 515, 1-12.

Dore, J., Church, M., Karl, D., Sadler, D., & Letelier, R. (2014). Paired windward and leeward biogeochemical time series reveal consistent surface ocean CO2 trends across the Hawaiian Ridge. *Geophysical Research Letters, 41,* 6459-6467.

Dore, J. E., Lukas, R., Sadler, D.W., Church, M.J., & Karl, D.M., (2009). Physical and biogeochemical

797 modulation of ocean acidification in the central North Pacific. *PNAS, 106*(30), 12235-
798 12240.
799
800 Dore, J., Lukas, R., Sadler, D., & Karl, D., (2003). Climate-driven changes to atmospheric CO2 sink
801 in the subtropical North Pacific Ocean. *Nature, 424*, 754-757.
802
803 Duarte, C. M., Regaudie-de-Gioux, A., Arrieta, J. M., Delgado-Huertas, A., & Agustí, S. (2013).
804 The oligotrophic ocean is heterotrophic. Annual Review of Marine Science, 5, 551–569.
805 https://doi.org/10.1146/annurev-marine-121211-172337
806
807 Ducklow, H. W., & Doney, S. C. (2013). What is the metabolic state of the oligotrophic ocean? A
808 debate. *Annual Review of Marine Science, 5,* 525–533. https://doi.org/10.1146/annurev-
809 marine-121211-172331
810
811 Emerson, S. (2014), Annual net community production and the biological carbon flux in the
812 ocean, *Global Biogeochem. Cycles*, 28, 14– 28, doi:10.1002/2013GB004680.
813
814 Emerson, S., Quay, P. D., Karl, D. M., Winn, C., Tupas, L., & Landry, M. (1997). Experimental
815 determination of the organic carbon flux from open-ocean surface waters. Nature, 389,
816 951–954. https://doi.org/10.1038/40111
817 Emerson, S., Quay, P. D., Stump, C., Wilbur, D., & Schudlich, R. (1995). Chemical tracers of
818 productivity and respiration in the subtropical Pacific Ocean. *Journal of Geophysical*
819 *Research, 100,* 873–887. https://doi.org/10.1029/95jc01333
820
821 Emerson, S., Stump, C., & Nicholson, D. P. (2008). Net biological oxygen production in the
822 ocean: Remote in situ measurements of O2 and N2 in surface waters. *Global*
823 *Biogeochemical Cycles, 22,* GB3023. https://doi.org/10.1029/2007GB003095
824
825 Fassbender, A.J., Sabine, C.L., & Cronin, M.F., (2016). Net community production and
826 calcification from 7 years of NOAA Station Papa Mooring measurements. *Global*
827 *Biogeochemical Cycles, 30,* 250-257.
828
829 Fassbender, A.J., Sabine, C.L., Cronin, M.F., & Sutton, A.J., (2017). Mixed-layer carbon cycling at
830 the Kuroshio Extension Observatory. *Global Biogeochemical Cycles, 31,* 272-288.
831
832 Fernández-Castro, B., Mouriño-Carballido, B., Benítez-Barrios, V. M., Chouciño, P., Fraile-Nuez,
833 E., Graña, R., Piedeleu, M., & Rodríguez-Santana, A. (2014). Microstructure turbulence
834 and diffusivity parameterization in the tropical and subtropical Atlantic, Pacific and
835 Indian Oceans during the Malaspina 2010 expedition. *Deep Sea Research Part I:*
836 *Oceanographic Research Papers*, *94*, 15-30.
837
838 Ferrón, S., Barone, B., Church, M.J., White, A.E., & Karl, D.M., (2021). Euphotic zone metabolism
839 in the North Pacific Subtropical Gyre based on oxygen dynamics. *Global Biogeochemical*
840 *Cycles, 35,* e2020GB006744. doi: 10.1029/2020GB006744

Firing, E., (1996). Currents observed north of Oahu during the first five years of HOT. *Deep Sea Research II, 43(*2-3), 281-303.

Follett, C. L., Dutkiewicz, S., Karl, D. M., Inomura, K., & Follows, M. J. (2018). Seasonal resource conditions favor a summertime increase in North Pacific diatom–diazotroph associations. *The ISME journal*, *12*(6), 1543-1557.

Gruber, N., & Sarmiento, J. L. (1997). Global patterns of marine nitrogen fixation and denitrification. *Global biogeochemical cycles*, *11*(2), 235-266.

Hamme, R. C., & Emerson, S. (2004). The solubility of neon, nitrogen and argon in distilled water and seawater. *Deep-Sea Research Part I: Oceanographic Research Papers, 51*, 1517–1528. https://doi.org/10.1016/j.dsr.2004.06.009

Hastenrath, S., & Merle, J. (1987). Annual cycle of subsurface thermal structure in the tropical Atlantic Ocean. *Journal of Physical Oceanography*, *17*(9), 1518-1538.

Ho, D. T., Law, C., Smith, M., Schlosser, P., Harvey, M., & Hill, P., (2006). Measurements of air-sea gas exchange at high wind speeds in the Southern Ocean: Implications for global parameterizations. *Geophysical Research Letters, 33,* L16611.

Humphreys, M. P., Lewis, E. R., Sharp, J. D., and Pierrot, D. (2022a). PyCO2SYS v1.8: marine carbonate system calculations in Python. *Geoscientific Model Development* 15, 15-43. doi:10.5194/gmd-15-15-2022.

Humphreys, M. P., Schiller, A. J., Sandborn, D. E., Gregor, L., Pierrot, D., van Heuven, S. M. A. C., Lewis, E. R., and Wallace, D. W. R. (2022b). PyCO2SYS: marine carbonate system calculations in Python. *Zenodo.* doi:10.5281/zenodo.3744275.

Johnson, G.C., (2001). The Pacific Ocean subtropical cell surface limb. Geophysical Research *Letters, 28*(9), 1771-1774.

Kara, A. B., Rochford, P. A., & Hurlburt, H. E. (2000). An optimal definition for ocean mixed layer depth. *Journal of Geophysical Research: Oceans*, *105*(C7), 16803-16821.

Karl, D. M. (1999). A Sea of Change: Biogeochemical Variability in the North Pacific Subtropical Gyre. *Ecosystems*, *2*(*3*), 181–214.

Karl., D. M., Christian, J. R., Dore, J. E., Hebel, D. V., Letelier, R. M., Tupas, L. M., & Winn, C. D., (1996). Seasonal and interannual variability in primary production and particle flux at Station ALOHA. *Deep Sea Research II,* 43(*2-3*), 539-568.

Karl, D., & Church, M. (2017). Ecosystem structure and dynamics in the North Pacific Subtropical Gyre: New views of an old ocean. *Ecosystems, 20,* 433-457.

Karl, D., & Church, M. (2018). Station ALOHA: A gathering place for discovery, education, and scientific collaboration. *Limnology and Oceanography Bulletin*.

Karl, D.M., Letelier, R.M., Bidigare, R.R., Björkman, K.M., Church, M.J., Dore, J.E., & White, A.E., (2021). Seasonal-to-decadal scale variability in primary production and particulate matter export at Station ALOHA. *Progress in Oceanography*. doi: https://doi.org/10.1016/j.pocean.2021.102563

Karl, D. M., & Lukas, R. (1996). The Hawaii Ocean Time-series (HOT) program: Background, rationale and field implementation. *Deep Sea Research Part II: Topical Studies in Oceanography, 43*(2-3), 129–156. doi:10.1016/0967-0645(96)00005-7

Keeling, C.D., Brix, H., & Gruber, N., (2004). Seasonal and long-term dynamics of the upper ocean carbon cycle at Station ALOHA near Hawaii. *Global Biogeochemical Cycles,* 18, GB4006.

Letelier, R.M., Karl, D.M., Abbott, M.R., Flament, P., Freilich, M., Lukas, R., & Strub, T., (2000). Role of late winter mesoscale events in the biogeochemical variability of the upper water column of the North Pacific Subtropical Gyre. *Journal of Geophysical Research, 105*(C12), 287723-28739.

Lee, K. (2001). Global net community production estimated from the annual cycle of surface water total dissolved inorganic carbon. *Limnology & Oceanography, 46*, 1287–1297. https://doi.org/10.4319/lo.2001.46.6.1287

Levitus, S. (1982). *Climatological atlas of the world ocean* (Vol. 13). US Department of Commerce, National Oceanic and Atmospheric Administration.

Liu, W. T., Katsaros, K. B., & Businger, J. A. (1979). Bulk parameterization of air-sea exchanges of heat and water vapor including the molecular constraints at the interface. *Journal of the Atmospheric Sciences*, *36*(9), 1722-1735.

Lueker, T. J., Dickson, A. G., & Keeling, C. D. (2000). Ocean pCO2 calculated from dissolved inorganic carbon, alkalinity, and equations for K1 and K2: validation based on laboratory measurements of CO2 in gas and seawater at equilibrium. *Marine Chemistry*, *70*(1-3), 105-119.

Lukas, R., & Santiago-Mandujano, F. (2008). Interannual to interdecadal salinity variations observed near Hawaii: Local and remote forcing by surface freshwater fluxes. *Oceanography*, *21*(1), 46-55.

McLaughlin, K., S.B. Weisberg, A.G. Dickson, G.E. Hofmann, J.A. Newton, D. Aseltine-Neilson, A. Barton, S. Cudd, R.A. Feely, I.W. Jefferds, and others, (2015). Core principles of the California Current Acidification Network: Linking chemistry, physics, and ecological effects. Oceanography 28(2), 160–169.

Monteagudo, M. M. (2016). *Planktonic foraminiferal faunal study and Mg/Ca-temperature calibration at the Hawaii Ocean Time-Series*. University of California, Santa Barbara.

Neuer, S., Davenport, R., Freudenthal, T., Wefer, G., Llinás, O., Rueda, M.-J., Steinberg, D. K., & Karl, D. M., (2002). Differences in the biological carbon pump at three subtropical ocean sites, *Geophys. Res. Lett.*, 29(*18*), 1885, doi:10.1029/2002GL015393.

Nickford, S., J.B. Palter, K. Donohue, A.J. Fassbender, A.R. Gray, J. Long, A.J. Sutton, N.R. Bates, and Y. Takeshita (2022). Autonomous Wintertime Observations of Air-Sea Exchange in the Gulf Stream Reveal a Perfect Storm for Ocean CO2 Uptake. Geophysical Research Letters, 49(5), e2021GL096805, https://doi.org/10.1029/2021GL096805.

Nicholson, S.-A., D.B. Whitt, I. Fer, M.D. du Plessis, A.D. Lebéhot, S. Swart, A.J. Sutton, and P.M.S. Monteiro. 2022. Storms drive outgassing of CO2 in the subpolar Southern Ocean. Nature Communications 13(1), 158, 10.1038/s41467-021-27780-w.

Nightingale, P. D., Malin, G., Law, C. S., Watson, A. J., Liss, P. S., Liddicoat, M. I., Boutin, J., & Upstill-Goddard, R. C. (2000). In situ evaluation of air-sea gas exchange parameterizations using novel conservative and volatile tracers. *Global Biogeochemical Cycles*, *14*(1), 373-387.

Orr, J. C., Epitalon, J. M., Dickson, A. G., & Gattuso, J. P. (2018). Routine uncertainty propagation for the marine carbon dioxide system. *Marine Chemistry*, *207*, 84-107.

Quay, P. D., Peacock, C., Björkman, K., & Karl, D. M. (2010). Measuring primary production rates in the ocean: Enigmatic results be- tween incubation and non - incubation methods at Station ALOHA. *Global Biogeochemical Cycles, 24,* GB3014. https://doi.org/10.1029/2009GB003665

Quay, P. D., Stutsman, J., Feely, R. A., & Juranek, L. W. (2009). Net community production rates across the subtropical and equatorial Pacific Ocean estimated from air-sea δ13C disequilibrium. *Global Biogeochemical Cycles, 23,* GB2006. https://doi.org/10.1029/2008GB003193

Quay, P., & Stutsman, J., (2003). Surface layer carbon budget for the subtropical N. Pacific: δ^{13}C constraints at Station ALOHA. *Deep-Sea Research Part I – Oceanographic Research Papers, 50*(9), 1045-1061.

970 Riser, S. C., & Johnson, K. S. (2008). Net production of oxygen in the subtropical ocean. *Nature,*
971 *451*, 323–325. https://doi.org/10.1038/nature06441
972
973 Sabine, C.L., Maenner Jones, S., Bott, R., Sutton, A.J., (2012). High-resolution ocean and
974 atmosphere pCO2 time-series measurements from mooring MOSEAN_158W_23N (NCEI
975 Accession 0100073). [complete dataset]. NOAA National Centers for Environmental
976 Information. Dataset. https://doi.org/10.3334/cdiac/otg.tsm_mosean. Accessed
977 11/15/2022.
978
979 Sabine, C., & Mackenzie, F., (1995). Bank-derived carbonate sediment transport and dissolution
980 in the Hawaiian archipelago. *Aquatic Geochemistry, 1,* 189-230.
981
982 Sabine, C. L., Mackenzie, F. T., Winn, C., & Karl, D. M. (1995). Geochemistry of carbon dioxide in
983 seawater at the Hawaii Ocean Time series station, ALOHA. *Global Biogeochemical*
984 *Cycles*, *9*(4), 637-651.
985
986 Santiago-Mandujano, F., Lukas, R., Murphy, D. J., & Larson, N. G. (2016). MicroCAT/SeaCAT
987 Sensor Calibration and Data Quality Control: Lessons Learned from 10 Years of WHOI-
988 Hawaii Ocean Time-Series Site (WHOTS) Mooring Deployments. *American Geophysical*
989 *Union*, *2016*, OD14C-2432.
990
991 Sonnerup, R. E., Mecking, S., & Bullister, J. L. (2013). Transit time distributions and oxygen
992 utilization rates in the Northeast Pacific Ocean from chlorofluorocarbons and sulfur
993 hexafluoride. *Deep-Sea Research Part I: Oceanographic Research Papers, 72*, 61–71.
994 https://doi.org/10.1016/j.dsr.2012.10.013
995
996 Sonnerup, R. E., Quay, P. D., & Bullister, J. L. (1999). Thermocline ventilation and oxygen
997 utilization rates in the subtropical North Pa- cific based on CFC distributions during
998 WOCE. *Deep-Sea Research Part I: Oceanographic Research Papers, 45*, 777–805.
999 https://doi. org/10.1016/S0967-0637(98)00092-2
1000
1001 Sprintall, J., & Tomczak, M. (1992). Evidence of the barrier layer in the surface layer of the
1002 tropics. *Journal of Geophysical Research: Oceans*, *97*(C5), 7305-7316.
1003
1004 Steinberg, D. K., Cope, J. S., Wilson, S. E., & Kobari, T., (2008). A comparison of mesopelagic
1005 mesozooplankton community structure in the subtropical and subarctic North Pacific
1006 Ocean. *Deep Sea Research Part II: Topical Studies in Oceanography*, *55*(14-15), 1615-
1007 1635.
1008
1009 Sulpis, O., Lauvset, S. K., and Hagens, M. (2020). Current estimates of K_1^* and K_2^* appear
1010 inconsistent with measured CO_2 system parameters in cold oceanic regions. *Ocean*
1011 *Science* 16(4), 847–862. doi:10.5194/os-2020-19.
1012
1013 Sutton, A. J., Sabine, C.L., Dietrich, C., Maenner Jones, S., Musielewicz, S., Bott, R., & Osborne,

J., (2012). High-resolution ocean and atmosphere pCO2 time-series measurements from mooring WHOTS_158W_23N in the North Pacific Ocean (NCEI Accession 0100080). [indicate subset used]. NOAA National Centers for Environmental Information. Dataset. https://doi.org/10.3334/cdiac/otg.tsm_whots. Accessed [11/15/2022].

Sutton, A.J., C.L. Sabine, R.A. Feely, W.J. Cai, M.F. Cronin, M.J. McPhaden, J.M. Morell, J.A. Newton, J.H. Noh, S.R. Ólafsdóttir, and others, (2016). Using present-day observations to detect when anthropogenic change forces surface ocean carbonate chemistry outside preindustrial bounds. Biogeosciences 13(17), 5065-5083, 10.5194/bg-13-5065-2016.

Sutton, A. J., Sabine, C. L., Maenner-Jones, S., Lawrence-Slavas, N., Meinig, C., Feely, R. A., Mathis, J. T., Musielewicz, S., Bott, R., McLain, P. D., Fought, H. J., & Kozyr, A. (2014). A high-frequency atmospheric and seawater pCO_2 data set from 14 open-ocean sites using a moored autonomous system. *Earth System Science Data*, *6*(2), 353-366.

Tomczak, M., & Godfrey, J.S., (2003). *Regional Oceanography: An Introduction*, 2nd ed., 390 pp., Daya, Delhi, India.

Uppström, L. R. (1974). The boron/chlorinity ratio of deep-sea water from the Pacific Ocean. *Deep-Sea Research* 21, 161–162. doi:10.1016/0011-7471(74)90074-6.

Venrick, E. L., (1993). Phytoplankton seasonality in the Central North Pacific: The endless summer
reconsidered. *Limnology and Oceanography,* 28(*6*), 1135-1149.

Wanninkhof, R. (1992), Relationship between wind speed and gas exchange over the ocean. *Journal of Geophysical Research, 97*(C5), 7373–7382.

Weiss, R. (1974), Carbon dioxide in water and seawater: The solubility of a non-ideal gas, *Marine Chemistry, 2*(3), 203–215.

Weller, R.A. & David, R.E., (1980). A vector measuring current meter. *Deep-Sea Research*, 27A, 565-582.

Williams, P. J. L. B., Quay, P. D., Westberry, T. K., & Behrenfeld, M. J. (2013). The oligotrophic ocean is autotrophic. Annual Review of Marine Science, 5, 535–549. https://doi.org/10.1146/annurev-marine-121211-172335

Wilson, S., Barone, B., Ascani, F., Bidgare, R.R., Church, M.J., del Valle, D.A., Dyhrman, S.T., Ferrón, S., Fitzsimmons, J.N., Juranek, L.W., Kolber, Z.S., Letelier, R.M., Martínez-García, S., Nicholson, D.P., Richards, K.J., Rii, Y.M., Rouco, M., Viviani, D.A., White, A.E., Zehr, J.P., Karl, D.M., (2015). Short-term variability in euphotic zone biogeochemistry and primary productivity at Station ALOHA: A case study of summer 2012.Global Biogeochemical Cycles, 29, 1145-1164.

Winn, C. D., Mackenzie, F. T, Carrillo, C. J., Sabine, C. L., & Karl, D. M., (1994). Air- sea carbon dioxide exchange in the North Pacific Subtropical Gyre: Implications for the global carbon budget. *Global Biogeochemical Cycles,* 8(*2*), 157-163.

Winn, C. D., Li, Y.H., Mackenzie, F. T., & Karl, D. M., (1998). Rising surface ocean dissolved inorganic carbon at the Hawaii Ocean Time-series site. *Marine Chemistry,* 60, 33-47.

Yang, B., Emerson, S., & Bushinsky, S. M. (2017). Annual net community production in the subtropical Pacific Ocean from in situ oxygen measurements on profiling floats. *Global Biogeochemical Cycles, 31*, 728–744. https://doi.org/10.1002/2016GB005545

Zhurbas, V., & Oh, I.S., (2004). Drifter-derived maps of lateral diffusivity in the Pacific and Atlantic Oceans in relation to surface circulation patterns. *Journal of Geophysical Research, 109*, C05015.